

REPORT DOCUMENTATION PAGE

AFRL-SR-BL-TR-01-

Public reporting burden for this collection of information is estimated to average 1 hour per response, including the time for reviewing the data needed, and completing and reviewing this collection of information. Send comments regarding this burden estimate or any reducing this burden to Washington Headquarters Services, Directorate for Information Operations and Reports, 1215 Jefferson Day Management and Budget, Paperwork Reduction Project (0704-0188), Washington, DC 20503

0655

1. AGENCY USE ONLY (Leave blank)		2. REPORT DATE		3. REPORT TYPE AND DATES COVERED Final Report 6-15-1997 to 6-30-2001	
4. TITLE AND SUBTITLE A Study of Rectangular Supersonic Jets Modified for Mixing Enhancement and Noise Reduction (AASERT97)				5. FUNDING NUMBERS F49620-97-1-0493	
6. AUTHOR(S) M. Samimy, C.W. Kerechanin II, and J.F. Kastner					
7. PERFORMING ORGANIZATION NAME(S) AND ADDRESS(ES) The Ohio State University Gas Dynamics and Turbulence Laboratory 206 West 18 th Avenue Columbus, Ohio 43210				8. PERFORMING ORGANIZATION REPORT NUMBER GDTL-AFOSR-12-01	
9. SPONSORING / MONITORING AGENCY NAME(S) AND ADDRESS(ES) AFOSR/NA 801 North Randolph Street, Room 732 Arlington, VA 22203-1977				10. SPONSORING / MONITORING AGENCY REPORT NUMBER	
11. SUPPLEMENTARY NOTES					
12a. DISTRIBUTION / AVAILABILITY STATEMENT Approved for public release; distribution unlimited				12b. DISTRIBUTION CODE AIR FORCE OFFICE OF SCIENTIFIC RESEARCH (AFOSR) NOTICE OF TRANSMITTAL DTIC DISTRIBUTION CODE REPORT HAS BEEN REVIEWED AND IS APPROVED FOR PUBLIC RELEASE LAW AFR 100-12. DISTRIBUTION IS UNLIMITED.	
13. ABSTRACT (Maximum 200 Words) This report presents the results of two experimental activities. Part I involves passive control of mixing and noise in a rectangular supersonic jet. Part II involves development and characterization of high amplitude and high bandwidth actuators for use in active control of high Reynolds and Mach numbers flows such as the jet in Part I. Nozzle trailing edge modifications were used in part I, which substantially enhanced mixing and reduced noise radiation in non-ideally expanded conditions, but did not significantly alter the mixing or noise for the ideally expanded flow condition. In part II, an in depth investigation of the Hartmann Tube was carried out. The effects of tube depth, separation distance between the tube and the nozzle, and the jet Mach number were explored. Experiments were also performed on a Hartmann Tube based Fluidic Actuator. Striking similarities were observed in the frequency content and amplitude of tonal frequencies in the global near-field pressure and far-field acoustic measurements, as well as, the flow results. Time traces of pressure in the tube were used to explain the major differences between the primary frequency of HT and the quarter-wave frequency. Flow visualization results showed a pulsating flow very rich in vortical structures.					
14. SUBJECT TERMS Passive Flow Control, Supersonic Jets, Mixing, Noise				15. NUMBER OF PAGES	
				16. PRICE CODE	
17. SECURITY CLASSIFICATION OF REPORT Unclassified	18. SECURITY CLASSIFICATION OF THIS PAGE Unclassified	19. SECURITY CLASSIFICATION OF ABSTRACT Unclassified		20. LIMITATION OF ABSTRACT Unlimited	

NSN 7540-01-280-5500

Standard Form 298 (Rev. 2-89)
Prescribed by ANSI Std. Z39-18
298-102

20020107 115

**A Study of Rectangular Supersonic Jets Modified for Mixing
Enhancement and Noise Reduction (ASSERT97)**

M. Samimy¹, C.W. Kerechanin II², and J.F. Kastner³

Gas Dynamics and Turbulence Laboratory

Department of Mechanical Engineering

The Ohio State University

Columbus, Ohio 43210

Final Technical Report

For the Air Force Office of Scientific Research

Grant AFOSR F49620-97-1-0493 (Dr. Thomas Beutner)

For the period of

June 15, 1997 to June 30, 2001

¹Principal Investigator, Professor and Director of GDTL

²Graduate Student; Currently with Applied Physics Laboratory, John Hopkins University

³Graduate Student

ABSTRACT

This report presents the results of two experimental activities. Part I involves passive control of mixing and noise in a rectangular supersonic jet. Part II involves development and characterization of high amplitude and high bandwidth actuators for use in active control of high Reynolds and Mach numbers flows such as the jet in Part I. Nozzle trailing edge modifications were used in part I, which substantially enhanced mixing and reduced the turbulent mixing and broadband shock associated noise radiation (by up to 12 dB for the underexpanded flow regime, and up to 7 dB for the overexpanded regime), but did not significantly alter the mixing or noise field for the ideally expanded flow condition. In part II, an in depth investigation of the Hartmann Tube (HT) was carried out to gain a better understanding of flow characteristics and the effects of various geometric parameters on its characteristics. The effects of tube depth, separation distance between the tube and the nozzle, and the jet Mach number were explored. Experiments were also performed on a Hartmann Tube based Fluidic Actuator (HTFA). Dynamic pressure measurements in the near field and microphone measurements in the far field provided temporal and spectral data. Instantaneous and phase-averaged images of the flow were obtained to explore the nature of turbulence structures within the flow. Striking similarities were observed in the frequency content and amplitude of tonal frequencies in the global near-field pressure and far-field acoustic measurements, as well as, the flow results. Time traces of pressure in the tube were used to explain the major differences between the primary frequency of HT and the quarter-wave frequency. Flow visualization results showed a pulsating flow very rich in vortical structures.

TABLE OF CONTENTS

I: Passive Control of Mixing and Noise in Supersonic Rectangular Jets.....	1
I.1 Introduction.....	1
I.2 Anechoic Chamber and Jet Flow Facility.....	1
I.3 Nozzle and Modifications.....	2
I.4 Acoustic Measurements.....	2
I.5 Experimental Results.....	3
I.6 Summary.....	6
II: Development and Characterization of Hartmann Tube Based Fluidic Actuators for High Speed Flow Control.....	7
II.1 Introduction.....	7
II.2 Experimental Setup.....	9
II.3 Results and Discussion.....	11
II.4 Summary.....	15
III: Acknowledgements.....	17
IV: References.....	18
V: Table.....	22
VI: Figures.....	23

Part I: Passive Control of Mixing and Noise in Supersonic Rectangular Jets

I.1 INTRODUCTION

The jet noise of aircraft has detrimental effects on the environment, causing economic hardships to those living in and around airports, and in the case of non-ideally expanded screeching jets, damage to the structure of the aircraft.¹ Proven methods for reducing jet noise do exist, but at great expense to the aircraft's overall performance, increasing the weight and drag of the vehicle. Researchers have been developing various noise reduction techniques, which work on the premise that by increasing the mixing of the jet flow with a bypass flow and thereby reducing the velocity, noise will be reduced.^{2,3} Other methods for increasing the mixing of jet flows with the ambient air, which have demonstrated the ability to decrease the overall radiated noise in both subsonic and supersonic jet flows include tabs or vortex generators,⁴⁻¹⁴ non-axially symmetric nozzles¹⁵⁻²⁰ and simple shaping of the nozzle trailing edge.^{18,20-26}

The main effect of a tab, which is similar in both subsonic and supersonic flows, is to generate a pair of strong streamwise vortices. These vortices entrain ambient air into the jet and substantially enhance gross mixing of the jet with the ambient fluid. The tabs have been shown to eliminate or reduce screech noise, to substantially reduce mixing and shock associated noise in lower frequencies, but to increase it in higher frequencies.^{4,5,8} Thrust penalties have been demonstrated for the tabbed nozzles, due to the partial blocking of the nozzle exit area.^{8,12,13}

Trailing edge modified nozzles have been recently examined for their ability to increase mixing and to decrease the far field noise.^{23,24,26} In underexpanded supersonic jet flows, streamwise vortices, generated by a spanwise pressure gradient over the modified trailing edges, caused a substantial increase in the mixing and a decrease in noise. An adverse pressure gradient within the nozzle for the overexpanded flow regime, caused flow separation within the nozzle with minimal mixing enhancements and did not affect the mixing noise, however the screech tones were substantially reduced. The ideally expanded flow regime exhibited no mixing increases or altered noise fields, when the modifications to the trailing edges were either on the splitter plate in half nozzles or on the extension plates of a full nozzle.^{23,24} Trailing edge modifications have also been shown to not affect the thrust, as they do not block the nozzle exit area.²⁴ The recent work on the noise field of supersonic rectangular jets with modified trailing edges was preliminary and qualitative, as the facility was not anechoic.²³ The objective of the current study was two fold. First, to design and build a modular anechoic chamber that could be used for simultaneous flow and acoustic measurements. Second, to use it to examine the far field noise effects of nozzle trailing edge modifications on an aspect ratio 3 Mach 2 nozzle in various flow regimes.

I.2 ANECHOIC CHAMBER AND JET FLOW FACILITY

To quantitatively test the trailing edge modified nozzles for their acoustic qualities, an anechoic test facility^{27,28} was designed and employed, which is located at the Gas Dynamics and Turbulence Laboratory of the Ohio State University. A unique ability of this chamber is its modular design, where as with very little modification to the structure itself, that is removing a block of wedges for camera access, simultaneous flow and acoustic measurements can be taken without sacrificing the acoustic qualities.^{29,30} The floor is removable for simplified camera setup inside the chamber, and also extending its capabilities to allow hemi-anechoic acoustic testing conditions. The chamber has a cutoff frequency of 250 Hz., provided by the acoustic wedges

from Eckel Industries, and was tested for compliance to the ANSI Standard S12.35 for the decay of sound pressure levels in an anechoic room. Eight microphone paths, extending radially from a sound source in the center of the room to various corners and walls of the chamber were employed to evaluate the attenuation capabilities of the anechoic wedges. Figure 1 displays the comparison of the measured sound pressure level (SPL) at increasing distances from the white noise source to that of the inverse radius squared law³¹ for a path perpendicular to one of the chamber walls. Notice in the figure that there was excellent comparison, within 1.0 to 1.5 dB, of the theoretical curve as required by the standard. This result is similar to those in the other seven paths.²⁸ Two four-stage compressors supply the air for the jet facility, which is filtered, dried, and stored in two cylindrical tanks with a total capacity of 42.5 m³ at 16.5 MPa. The air is delivered to the laboratory through a 10.2 cm (4 in) diameter main line, with a 5.1 cm (2 in) diameter line providing air to the jet. This line passes through a pressure regulator, which is controlled by the user, who sets a specified pressure in the stagnation chamber. The air is expanded through a transition cone from the supply line to a 24.1 cm diameter pipe that is 91.4 cm long for flow conditioning. The air passes through a perforated plate (37% porosity), two mesh screens, and finally converges through a transition cone to a 6.0 cm pipe that is 40.6 cm long. After passing through this pipe, it enters an aspect ratio 3 rectangular nozzle, which is positioned so the major axis is vertical. The nozzle is attached to the pipe by an adapter, which takes the circular pipe cross-section smoothly down to the nozzle shape.

I.3 NOZZLE AND MODIFICATIONS

The aspect ratio 3 Mach 2 rectangular nozzle used in the present experiments was the same nozzle used in the previous studies,^{24,26} having a Reynolds number on the order of 1.3×10^6 . The nozzle dimensions are 0.95 cm high and 2.86 cm wide (3/8 inches by 1-1/8 inches). The equivalent diameter, the exit diameter of a circular nozzle with the same exit area, D_{eq} , for the nozzle was 18.6 mm (0.733 inches). The nozzle was designed for a nominal Mach number of 2.0, but the measured Mach number was 1.93. The modifications are made on the trailing edge extensions, to allow the flow to reach full expansion before approaching the cutouts, Fig. 2(a). In earlier results based on flow visualization and mixing and preliminary acoustic measurements,^{23,24} four cutouts shown in Fig. 2(b) showed superior mixing and acoustic performance in comparison with other types of cutouts. In the current experiments, these four cutouts (total of eight modified nozzles) were tested against a baseline case at three flow conditions of ideally expanded ($M_j = 2.0$), overexpanded ($M_j = 1.75$) and underexpanded ($M_j = 2.5$). The nozzle-naming scheme will use the abbreviations introduced in the figure, where the baseline nozzle will be called BB and the modifications as RC (Rectangular Center cutout), RS (Rectangular Side cutout), OC (Oblique Center cutout) and OS (Oblique Side cutout).

I.4 ACOUSTIC MEASUREMENTS

Microphone Placement

Far-field acoustic measurements were carried out, using three 1/4-inch condenser microphones, B & K type 4135, with a type 2670 preamplifier, and two type 5935 dual microphone amplifying power sources. Two of the three microphones were positioned along the minor axis, with one located on the major axis of the nozzle, in a plane normal to the jet at downstream angles of 90°, 60° and 30°, measured from the jet axis. The microphones were mounted from the wedges on the walls and floor of the chamber. Figure 3 displays the microphone setup and nozzle orientation. The microphones were placed in the far field, 40 equivalent jet diameters (74.5 cm) from the nozzle axis.

Data Acquisition

Acoustic data for the three microphones, at the three measurement angles, for the nine nozzles while running at the three flow conditions, for a total of 81 data sets, were gathered using a National Instruments PC-416 Analog-to-Digital board, with a sampling rate of 190 kHz. The Labview data acquisition program sampled 100 blocks of 8192 points for each microphone, with a total sampling time of 4.31 seconds, and saved the data to the hard disk of a Pentium III personal computer. The frequency resolution or bandwidth is 23.2 Hz. The signals from the microphones were passed through a low pass frequency filter, DL Instruments model 4302, set to a cutoff frequency of 125 kHz. This was done to remove any high frequency anomalies from the microphones and to eliminate any potential aliasing. Calibration of the equipment was completed using a B & K type 4231 acoustical calibrator before each set of measurements ensuring that the data being gathered was consistent with changes in temperature and humidity. During testing, a high frequency (> 50 kHz) anomalous signal was noticed. To remedy this, the protective microphone screens were removed.

Data Reduction

The acoustic data was averaged using an in house Fast Fourier Transform program, based on the signal processing toolbox of Matlab, to obtain an averaged spectrum for each data set. The overall sound pressure level (OASPL) was then calculated by logarithmically adding the SPL for each frequency.

The frequency data was also scaled to an actual sized nozzle having an operating temperature of 800 K and a nozzle exit diameter of 0.3 m. This was accomplished by using the Strouhal number similarity, which shows that the ratio of the actual and experimental frequencies to depend on the operating temperature of the jets and equivalent diameters of the nozzles.²⁸ The scaling factor was found as

$$f_{actual} = (0.1033)f_{experimental} \quad (1)$$

The operating temperature of the jet was taken to be 288 K. The scaled data was then converted to the third octave band, between the center frequencies of 50 and 8000 Hz, and the perceived noise level (PNL) was calculated.¹ The first step was to convert all decibel levels at every frequency to a noys decibel value, which corresponds to the annoyance weightings applied to certain decibel amplitudes at specific frequencies. Then, using¹

$$N = 0.85n_{max} + 0.15 \sum_{i=1}^{23} n \quad (2)$$

$$PNLdB = 40 + \frac{10}{\log_{10} 2} \log_{10} N \quad (3)$$

where N is the total perceived noise, n is the perceived noise, and n_{max} is the maximum value of n, the PNL was in terms of PNLdB or noys. The noys were then logarithmically added to obtain an overall value, much like the OASPL.

1.5 EXPERIMENTAL RESULTS

The experimental results presented here are only a small fraction of the data detailed in reference 28. To understand the effects of the trailing edges on the noise, the effects of the modifications

on the flow field must first be examined. The mixing region of the jet at a cross section 1 equivalent jet diameter downstream of the nozzle exit is visualized in Fig. 4 using condensed water particles, generated during the mixing process of the entrained moist and warmer ambient air with the cold and dry jet air.²⁴ These images illustrate the overall effects of the various trailing edges on the jet in different flow regimes. In the $M_j = 2.5$ case, the addition of the modifications to the nozzle generates a spanwise pressure gradient on the cutouts that induces streamwise vortices. The side cutout nozzles, OS and RS, induce "kidney" type vortices that entrain ambient air into the jet as indicated by the arrows, and the center cutout nozzles, OC and RC, induce "mushroom" type vortices that eject the jet fluid into the ambient. These vortices substantially increase the mixing in the shear layer.²⁴ For the overexpanded flow regime, $M_j = 1.75$, a slight mixing increase was noticed, but the formation of an adverse pressure gradient within the nozzle caused flow separation and prevented the formation of streamwise vortices. The ideally expanded case, $M_j = 2.0$, saw no induced vortices and thus no mixing increase. Details of the flow field results and discussion can be found in references 24 and 26.

Underexpanded Spectra

Figure 5 displays the spectra for the four modifications as compared to the BB case, showing that the far field acoustic radiation was greatly reduced at 30° , over most of the spectrum, up to 12 dB. In this figure, for ease of comparison, each spectrum is upshifted by 20 dB, the first with respect to the BB, and a smoothed (Butterworth filtered) BB spectrum is overlaid on each shifted modification spectrum. Notice that the nozzle modifications, OC, OS and RC have the greatest decrease in the noise over the entire range from 1.5 to 80 kHz, as does the RS nozzle modification, but with less of a drop in amplitude for the higher frequencies. Since the turbulent mixing noise due to large scale structures is dominant at 30° ,^{32,33} the drop in noise could possibly be due the enhanced mixing from the streamwise vorticity and thus a reduction in the overall jet velocity.

Further investigation into the mixing processes of the nozzles could explain the behavior of RS in high frequency range in comparison with other nozzles. Figure 6 displays the normalized mixing area, calculated from the flow visualization results, for 4 different downstream locations, x/D_{eq} , where D_{eq} is the equivalent nozzle diameter and x is the distance downstream from the nozzle exit.²⁴ Looking at this figure, the RS nozzle modification, which entrains ambient air into the jet, is seen to have a strong early mixing, but to lose its strength further downstream, due to the destructive interaction that are taking place between the growing kidney type vortices. OC, OS and RC nozzle modifications, are seen to have a low to mid early mixing area, which is gradually growing in the downstream direction. When comparing Figs. 5 and 6, the interaction of the large-scale streamwise vortices in the RS case, produces large-scale structures cascading to smaller scale structures, much farther upstream, in comparison to the other cases. This produces high frequency noise, which could cause the increase in the amplitude of the RS spectrum in Fig. 5 above 10 kHz.

For the 60° location, there was substantial noise reduction in frequencies above 10 kHz, for all cases, except RS, and a slight increase in lower frequencies.^{27,28} For the 90° location, there was some changes between 4 and 10 kHz, a slight decrease in amplitude and shift in frequency.^{27,28}

Ideally Expanded and Overexpanded Spectra

Due to the lack of any measurable changes in the mixing for various nozzles in comparison with the BB nozzle in the ideally expanded flow regime, Fig. 4, there was also a lack of any change in the far field radiated noise in any of the three angles investigated. Figure 7 displays a sample data set for the 30° location. The overexpanded case had a slight increase of mixing from the BB

nozzle, as shown in Fig. 4, which accounts for some reduction in the low frequency turbulent mixing noise for the 30° location, especially for OC and RC nozzles.^{27,28} The screech tones were greatly affected by the nozzle modifications for the 90° location.

For the overexpanded flow condition, asymmetrically modified nozzles, Fig. 8, the screech is reduced in some case, RS, and practically eliminated, in some others, OS, RC and OC. This was caused by the breakup of the symmetry of the shock cells about the major axis of the nozzle, thus causing a diminished shock strength and acoustic feedback. The broadband shock associated noise is also reduced for the RC and OC nozzle modifications, with only slight reductions for the other two cases. The mixing noise was also reduced up to 7 dB for all modifications in the 2 to 10 kHz range.

The symmetrically modified (double side) nozzles for the overexpanded flow regime, Fig. 9, can be seen to have increased screech noise over the BB nozzle for the RS, RC and OC cases, with still diminished screech noise occurring in the OS nozzle. The return of the screech noise can be attributed to the symmetry of the nozzle. All of the nozzles, except for OS, exhibit an upshifted screech frequency. The broadband shock associated noise, which saw a decrease for the RC and OC nozzle in Fig. 8, increase in Fig. 9 to over the BB nozzle, causing increased high frequency noise, much like that seen in the tabbed nozzle cases. In this instance, the increase in the high frequency noise appears to be caused by the increased screech noise in the nozzle. For the RS and OS modifications, there was negligible change in the broadband shock associated noise.

The primary screech harmonic for the BB nozzle is 7600 Hz, with RS upshifting its primary harmonic to 8100 Hz, and RC and OC upshifting to 11 kHz, and OS downshifting to 7100 Hz. The screech tone radiation frequency has been shown to depend on the spacing of the shock cells.³⁴ Applying the following equation³⁵

$$L_{ss} = \frac{cM_c}{f_f(1+M_c)} \quad (4)$$

where L_{ss} is the shock cell spacing, c is the speed of sound in the ambient, M_c is the convective Mach number and f_f is the frequency of the primary screech harmonic, the effects of the modifications on the flow become clearer. For the BB nozzle, $L_{ss \text{ at } 7600} = 20.3$ mm, for RS, $L_{ss \text{ at } 8100} = 19.0$ mm, for RC and OC $L_{ss \text{ at } 11000} = 14.0$ and for OS $L_{ss \text{ at } 7100} = 21.7$ mm. The double side modifications RS, RC and OC cause the shock cells spacing to become reduced in size creating a higher frequency of radiation than the BB nozzle, and possibly creating a stronger shock cell structure. The OS modification for both single and double-sided nozzles has an elongated shock cell structure, thus a lower frequency of radiation and possibly a weakened shock cell structure.

Overall Sound Pressure Level

The OASPL displays the changes in the overall radiated noise due to the modifications. For the underexpanded flow regime, Fig. 10 displays the results for the OASPL calculated at the three microphone locations for spectra presented in Fig. 5. Notice that the noise has been greatly reduced for both sides of the nozzle, and for all modifications. In the sideline microphone location, microphone 2, only the nozzles that entrain ambient air into the jet, RS and OS, and thus flatten the mixing layer on the sideline, as in Fig. 4, tend to decrease noise up to 5 dB. The OASPL changes at 60° and 90° were relatively small.^{27,28}

The overexpanded OASPL results for the 90° microphone location are similar to the spectra, where as the noise being slightly reduced and increased, in the asymmetrically and symmetrically modified nozzles, respectively. For the 30° microphone location, both type of nozzles showed reduction in the OASPL. The ideally expanded OASPL plots also have the same characteristics as the spectra, where as there is no change from the BB nozzle.²⁸

Perceived Noise Level

The PNL amplitude levels for the scaled nozzle were greater than that of the OASPL amplitude values, most likely due to the heavy weighting of the higher frequencies. Fig. 11 displays the underexpanded case examined in this paper. Notice that the reductions seen from the creation of the streamwise vortices are still present, and of the same magnitude as the OASPL values. For the overexpanded cases, the PNL had deviations from the BB nozzle less than those did in the OASPL cases.²⁸ The ideally expanded case did not have any deviation, as would be expected.²⁸ Conclusions that could be drawn from the PNL is that the actual sized nozzle could radiate at a higher decibel level than that of the test nozzle, with less reductions in the screech noise, but still major reductions in the downstream turbulent mixing noise.

1.6 SUMMARY

The acoustic experiments for a Mach 2 rectangular jet with trailing edge modifications have been carried out in the newly designed anechoic chamber to investigate the effects of the modifications on the acoustic far field. Measurements were conducted in the 90°, 60° and 30° degree directions from the jet axis, in order to capture the screech and broadband shock associated noise in their dominant radiation direction, upstream, and to measure the effects of the turbulent mixing noise and possible Mach wave radiation effects in their dominantly downstream radiation direction. Three microphones on a plane normal to the jet axis, two placed on the minor axis and one on the major axis of the nozzle, were used to measure the effects that the single (asymmetric) and double side (symmetric) trailing edge modifications had on the far field noise.

In the underexpanded flow regime, the greatest effects of the modifications are in creation of the streamwise vortices, which reduce the acoustic far field radiation by up to 12 dB for both the single and double side modified nozzles. In the overexpanded flow regime, the screech tones were reduced or eliminated for the single side modified nozzles, caused by a disruption in the symmetry of the nozzle about the major axis, and a weakened feedback loop. The OS modification also caused an elongation of the shock cell structure, dropping the screech frequency by 500 Hz. The double side modified nozzle in the overexpanded flow regime had an increase in screech noise over the BB for all nozzles except the OS case. This was caused by the symmetry in the nozzle about the major axis, and a strengthening of the shock structure by a compression of the cells, demonstrated by looking at the upshift in the screech frequency. OS still exhibited reduced screech noise, and an elongation of the cell structure. The perfectly expanded case was not affected by the modifications.

The OASPL and the PNL were calculated for a test nozzle and a scaled nozzle, respectively. Both had similar reductions in the turbulent mixing noise for the 30° measurement location in comparison with the BB case. The ideally expanded case was also similar, as there were no deviations from the BB. For the overexpanded flow regime, the OASPL had reduced screech noise evident in the single side modified nozzle, with increased screech noise in the double sided modified nozzle. The PNL results still exhibited these decrease, but in a reduced amount. There was also a 10 dB difference between the OASPL and the PNL results, possibly signifying that the overall noise for the larger nozzle would be greater, however the reductions in the overall mixing noise would still be present in the underexpanded operating conditions.

Part II: Development and Characterization of Hartmann Tube Based Fluidic Actuators for High Speed Flow Control

II.1 INTRODUCTION

Hartmann Tube

A pitot probe is a simple device that has been used for stagnation pressure measurement since the early days of gas dynamics as an engineering and scientific subject area. It is a tube with one open end that is directly facing the flow and the other end is connected to a pressure gauge and thus closed off. If the tube is used in a subsonic flow, the flow isentropically decelerates and reaches zero velocity on a streamline approaching the tube; hence the stagnation pressure of the flow is measured. If the flow is supersonic, a bow shock is formed in front of the tube, and the measured stagnation pressure is that of the flow after the shock wave, which is lower than the stagnation pressure before the shock wave, due to the highly dissipative nature of the shock wave. When Hartmann used a pitot tube in an underexpanded jet, he obtained an almost sinusoidally varying stagnation pressure along the centerline of the jet (Hartmann and Trolle⁴⁰), which is expected due to the now well-known compression-expansion pattern in such a flow. However, Hartmann noticed that every time he placed the pitot probe within a compression region of the jet, it resulted in a high intensity, pure tone noise. Hartmann called these regions 'intervals of instability.' It was later discovered that the tone resulted from the interaction of the jet with the cavity of the pitot probe.

Once the pitot probe is placed within the compression region of an underexpanded jet, the tube begins to draw fluid in and compression waves are created at the tube entrance that traverse towards the closed end of the tube (the beginning of compression phase and the overall cycle). The compression waves are reflected at the end wall as compression waves, which move back toward the entrance of the probe. When these waves reach the open end, they are reflected back into the tube as expansion waves (the end of compression phase and the beginning of expansion phase). At this time, the pressure within the tube has risen above the local jet pressure. The tube therefore starts relieving itself of the high pressure by ejecting some of the fluid accumulated within the tube. The expansion waves traveling through the tube are reflected on the back wall as expansion waves. Once these waves reach the open end of the tube, they are reflected as compression waves (the end of the expansion phase and the cycle). Once again, the pressure in the tube is sufficiently low to allow the inflow of fluid into the tube. Thus, the expansion phase and the overall cycle are complete and the compression phase of the cycle begins again.

The time (Δt) for this cycle, or the frequency (f) can then be calculated from:

$$\Delta t = \frac{1}{f} = \frac{L}{u_{ic}} + \frac{L}{u_{rc}} + \frac{L}{u_{ie}} + \frac{L}{u_{re}} \quad (5)$$

where L is the depth of the tube, u is the absolute velocity of the wave (velocity with respect to the tube), the subscripts i for incident, r for reflected, c for compression, and e for expansion. For accurate calculation of f using Equation (5), the speed of the individual waves along with the flow velocity within the tube has to be known. An approximate, but convenient way to predict the frequency is to assume that all the waves are Mach waves and thus travel with the local speed of sound and the flow velocity within the tube is negligible. With these two assumptions $u_{ic} = u_{rc} = u_{ie} = u_{re} = c$, and Equation (5) becomes the quarter wave frequency equation:

$$\Delta t = \frac{1}{f_{qw}} = \frac{4L}{c} \quad (6)$$

where c is the speed of sound. Raman et al.⁵⁶ have shown that this formula is fairly accurate for long tube depths, while it over predicts the frequency for short tube depths.

All that has been described so far is what is happening inside the tube. For flow control purposes the nature of the pulsating jet out of this nozzle-tube system is most relevant. This pulsating jet runs in phase with the compression and expansion phases as described above. During the compression phase, the pulsating jet will have minimum flow as the air from the nozzle is being compressed into the tube. During the expansion phase, the pulsating jet will have maximum flow as the air from the nozzle is pushed back by the flow emitting from the tube. The strength of the flow exiting the tube, in comparison with the nozzle flow, will determine the direction of the pulsating jet.

Following Hartmann's initial work on the Hartmann tube, much work was carried out to explore its characteristics. By using the hydraulic analogy, researchers (Morch⁵¹, Solomon⁵⁸, and Iwamoto and Deckker⁴⁴) have been able to better characterize the shock structures and the pressure field present within the flow. Iwamoto and Deckker⁴⁴ used the hydraulic analogy to demonstrate the existence of a low-pressure region near the tube entrance. Such a low-pressure region is necessary for oscillations in an underexpanded HT.

Brocher³⁶ described the wave characteristics present within the tube by showing how oscillations within the tube are able to grow or be kept from growing due to a momentum deficit along the jet centerline. This shed light for example on why a needle should be used on the axis of a HT with a converging-diverging (C-D) nozzle. Brocher³⁶ and Raman et al.⁵⁴ have shown that when the HT with a C-D nozzle is used, it requires a much larger separation distance between the nozzle and the tube in comparison with a HT with converging nozzle. This can make a HT with a C-D nozzle somewhat less ideal for an actuator because the larger separation distance would result in a less compact actuator. Raman et al.⁵⁴ added a cylindrical shield between the nozzle and tube, covering a large portion of this open surface. This modification converted the HT to a fluidic injector/actuator.

The shape of the Hartmann Tube was changed into a stepped cavity by Sprenger⁵⁹ to enhance the heating characteristics of the tube primarily by increasing irreversibilities present within the tube. Kawahashi et al.⁴⁷ and Brocher and Ardisson³⁷ present good summaries of the use of a stepped tube. This alteration of the HT gave way to applications where the end wall was used as a high frequency pneumatic igniter (Marchese et al.⁵⁰). Raman et al.⁵⁶ tested both a stepped tube and a conical tube. The results showed an increase in frequency for both the stepped and conical tubes. The frequency range was 46 kHz for a standard cylindrical tube, but was on the order of 7-11 kHz for both the conical and stepped tubes. An amplitude comparison amongst the three configurations showed minor variation on the order of 1-3dB in the amplitude of far-field noise.

Flow Control

It has been known for decades that large coherent structures play major roles in entrainment, mixing, and noise generation in free flows (Crow and Champagne³⁹, Brown and Roshko³⁸, Winant and Broward⁶³, Kibens⁴⁸, and Ho and Huang⁴²). Active control of these structures is a very effective and desirable way of manipulating these processes (Kibens⁴⁸, Ho and Huerre⁴³, Parekh et al.⁵³, Kibens et al.⁴⁹). The conventional method of low amplitude forcing at the instability frequencies of the flow has not been successful in high-speed flows for two reasons. First, instability frequencies in a typical laboratory flow are very high. For a typical 1-inch

diameter axisymmetric jet of 400 m/s velocity, the shear layer instability is on the order of 80 kHz, and the jet column frequency is 3 to 10 kHz. Second, high Reynolds number flows possess high dynamic loading and noisy environment, which require high amplitude forcing. The lack of the availability of actuators with high bandwidth and high amplitude has been one of the main obstacles in active control of high-speed flows.

Three promising events have taken place in recent years that show the potential of such actuators in high-speed flow control. First, it has been shown that shear layers of a high Reynolds number jet can be forced at jet column frequency, but the required forcing amplitude is much higher than that used traditionally (Kibens et al.⁴⁹). Second, high Reynolds number shear layers can also be forced with frequencies much higher than their instability frequencies through the use of higher amplitudes (Stanek et al.^{60, 61}). This work was performed in a cavity flow with strong resonance. It remains to be seen whether this can be done in a shear layer with a broadband spectrum. The third event is the recent development of high bandwidth and amplitude fluidic actuators based on the HT (Raman et al.^{54, 56}). In fact, Stanek et al.^{60, 61} have already used these actuators in a cavity flow, and Raman and Kibens⁵⁵ have used them on an impinging jet.

The frequency characteristics and the effects of various variables such as tube depth, the distance between the nozzle and the tube, and the jet Mach number (or the nozzle pressure ratio) have been explored by many researchers for the HT and by Raman et al.⁵⁶ for the actuators based on the HT. However, not much is known on the flow out of either one. This kind of information is important when the fluidic actuator is used for flow control. The main objective of the current work is to provide some information on flow characteristics, along with additional information on other aspects of the actuator.

II.2 EXPERIMENTAL SETUP

Facility

A HT was constructed that allowed for the adjustment of various parameters. Figure 12 shows a schematic of the HT where the tube diameter (d), the separation distance (Δx), and the tube depth (L) are all labeled. The diameter of the nozzle and the tube were both equal to 6mm for all experiments reported here. Figure 13 shows a photograph of the setup with the nozzle on the left and the tube on the right. The tube was constructed with a moveable piston to allow for the depth of the tube to be varied. The piston was sealed in the tube with an o-ring. The piston was capable of changing the depth of the tube from $1d$ all the way up to $15d$. This gives an approximate frequency range (Eqn. 6) from 0.95 kHz for $15d$ up to 14.3 kHz for $1d$. This whole range was not realized experimentally, especially towards the higher end where the maximum frequency reached was 9.4 kHz. As will be discussed later, the maximum amplitude occurs when $\Delta x = 1d$. Since for maximum frequency $L = d$ and since $f \sim L^{-1}$, to achieve higher frequency, one needs to use a nozzle and tube with smaller diameter.

Another parameter that was varied in the current set up was the separation distance between the nozzle and the tube. A Newport Linear Stage with a micrometer was used to precisely control the separation distance. The setup allowed for the separation distance to be varied between $1d$ and $3d$. By varying the separation distance, the entrance of the tube could be varied with respect to the shock cell structures of the underexpanded jet for a given jet Mach number.

When the HT is used as a fluidic actuator, a cylindrical shield can be placed between the nozzle and the tube (Raman et al.⁵⁴). This shield directs all the flow to exit from one side, which allows injection into a flow to be controlled. Such a HT with a shield (HTFA) was designed to explore

its characteristics and to compare and contrast with those of the HT. A photograph of the current HTFA is shown in Figure 14. The shield in the current set up is a permanent part of the HTFA. A separation distance (Δx) of 8mm between the nozzle and tube was used in the current set up. Similar to the HT setup, the nozzle and tube diameters were both 6mm for the HTFA. To vary the depth of the tube for the HTFA, caps were designed that attached directly to the tube. This allowed tube depths of $1d$, $2d$, and $3d$ to be studied. Experiments were performed on the HTFA to explore its characteristics. The results of these experiments, as will be discussed later, showed that the HT and HTFA exhibit similar frequency characteristics, but different amplitude characteristics. The air supplied to the converging nozzle was controlled by a Grove (Model 15LH) needle valve. This set up allowed a pressure ratio up to 5.75 giving a jet Mach number (M_j) as high as 1.8. A static pressure tap was placed at the exit of the nozzle to accurately measure the jet Mach number. The nozzle had an exit diameter of 6mm, which gave a mass flow of 0.0126 kg/s when operating in the ideally expanded regime and a mass flow of 0.0382 kg/s for an M_j of 1.8.

Acoustic and Pressure Measurements

Far-field acoustic measurements were made 50 jet diameters away from the nozzle exit using a $\frac{1}{4}$ " Bruel and Kjaer (B&K) Model 4135 microphone. The microphone was calibrated with a B&K Model 4231 sound level calibrator. The acoustic signal was low pass filtered at 125 kHz and a Dattel PC416 A/D board was used to sample it at 400 kHz. The data acquisition process was controlled using Labview. Instantaneous near-field pressure data were acquired using a dynamic Endevco pressure transducer (Model 8514-10) attached on the tube 1.2 mm from the open end. The Wheatstone bridge on the pressure transducer was powered with a 10V excitation provided by an Ectron model 563F signal conditioner. The same signal conditioner was used to amplify the signal before being sent to the Dattel PC 416 A/D board. The low pass filter and sampling rate were the same to those of the acoustic signal.

The frequency content of the flow field between the nozzle and tube was explored using a Uniphase (Model 106-1) He-Ne CW Laser. The laser beam of about 1 mm diameter was passed through the flow field, normal to the jet centerline and half way between the nozzle and tube before reaching a photodiode on the other side. The photodiode measured the intensity of the light and how it varied with time due to the density variations in the flow. This gave a line-of-sight averaged measurement of flow variations affecting the laser beam intensity over the laser path within the flow. As with the microphone and pressure transducer, the data was acquired through Labview using the Dattel A/D board.

Once all the data was acquired and saved, FFT of the microphone, pressure transducer, and the photodiode signals were performed on 100 blocks containing 8192 data points per block by using Matlab. In order to compare amplitudes, the sound pressure level (SPL) was computed for the microphone while the amplitude for the pressure transducer and photodiode were normalized by the corresponding rms value of the signal for $L=1d$ and $\Delta X=1d$. The signal had the highest amplitude at this case and therefore was used as a benchmark against other tube depths and separation distances.

Flow Visualization

Flow visualization was performed using laser sheet illumination. The laser beam was provided from a Continuum Powerlite 8010 Nd:YAG operating at a wavelength of 532 nm. The maximum repetition rate of the laser was 10 Hz and the pulse duration was 9 ns. With only a 10 Hz repetition rate, the laser could not provide time-correlated images. Instead, the laser was phase-locked with the far-field acoustic signal of the HT. As will be discussed later, this far-field signal

had a distinct primary frequency when the entrance of the HT tube was within a compression region. In order to obtain phase-locked images, a real time signal from a B&K microphone was sent to a PC-T10-10 timing board after it was low and high pass filtered to obtain a smoothly varying signal. The filtering allowed for the removal of any harmonics that could interrupt the triggering program. The signal was amplified to have magnitudes recognized by the timing board. The timing program was triggered by the rising edge of the signal once it was greater than 5V. Once the triggering had taken place, a TTL signal was sent to the laser that was also synched with a digital camera.

The laser was used to form a streamwise sheet that illuminated the centerline of the jet/tube of the HT and the HTFA. The tube and nozzle were painted black or anodized to reduce scattering of the laser light from the solid surfaces. The laser was synched to a 14-bit Princeton Instruments ICCD camera through a Princeton Instruments PG-200 programmable pulse generator. The camera was placed orthogonal to the plane of the laser sheet. An extension tube was placed between the camera and the lens to allow focusing at a closer distance. The camera had a resolution of 588 by 384 pixels and was also intensified during experiments to improve signal intensity.

Seeding of the flow was accomplished using acetone injected approximately 11 m upstream of the nozzle exit. This long distance is necessary to allow acetone to evaporate and mix with air before entering the nozzle. After the flow was injected with acetone it was passed through a chamber to achieve better mixing between the flow and acetone. The flow visualization technique relies on Mie scattering of laser light by acetone particles condensing during flow expansion within the nozzle. For all cases, 60 instantaneous images were taken during 8 equally spaced phases of one cycle at the primary frequency. These 60 images were used to obtain phase-averaged images.

II.3 RESULTS AND DISCUSSION

Tube Depth

The depth of the tube has multiple impacts on the results of the HT. Hartmann⁴¹ showed that both the frequency and amplitude peaked around a tube depth of $1d$. For the present study, the effects of tube depth will be presented and discussed in detail. First, the quarter wave frequency (Eqn. 2) will be compared with the experimental results, and then the reasons for the observed differences will be discussed in the context of the near-field pressure time traces. The time traces give a good description of the differences between the compression and expansion phases. Finally, the impact of tube depth on amplitude will be briefly explored.

Figure 15 shows the magnitude of the primary far-field acoustic frequency of the HT versus M_f for various tube depths (L). As will be discussed later, the tonal frequency contents of the far-field acoustic and near-field pressure are identical. The quarter-wave frequency (f_{qw}) for each tube depth is also shown. It is clear from the figure that as the tube depth is increased, the frequency is getting closer to the quarter-wave value. Raman et al.⁵⁴ presented similar results where longer tube depths produced frequencies much closer to the quarter-wave prediction than shorter tubes. Table 1 further supports this by showing the minimum and maximum measured frequencies in comparison with the quarter-wave frequency for each tube depth. For a tube depth of $1d$ the actual frequency differs from the quarter wave frequency by 35% to 49%, while for a tube depth of $6d$, the difference is only from 8% to 17%.

To help understand the reason for these differences, it is beneficial to look at the time trace of one cycle. A time trace can be used to show the difference between the compression and expansion

phases of the HT. Brocher³⁶ briefly looked at this issue. Figure 16 shows a time trace of the pressure for two tube depths of $L=1d$ and $L=3d$. For the smaller tube depth, the duration for the compression and expansion phases is approximately the same. On the other hand, for the longer tube depth, the compression phase takes much longer than the expansion phase. The result of this is that the HT is generating a nearly sinusoidal near-field pressure only when the tube depth is on the order of $1d$. Table 1 shows the percentage of duration for the compression and expansion phases in a cycle for various tube depths. The compression phase increases from 52% of the cycle for $1d$ all the way to 64% for $6d$.

Using the phase information from Fig. 16 and the tube depth, the average absolute velocities for compression and expansion phases could be calculated. Figure 17 shows these velocities along with the average wave speed over the entire cycle for various tube depths. The average compression wave speed was calculated from the time it takes the pressure to rise from trough to peak, and the average expansion wave speed was found from the time taken to go from peak to trough. The average wave speed for the expansion wave is the same as the compression wave for tube depths of $1d$. However, as the tube depth is increased, the expansion wave speed increases faster than the compression wave speed. One noticeable result is that the average wave speed is much lower than speed of sound for the $1d$ case, but approaches the speed of sound for larger tube depths.

The results presented in Figures 16 and 17 provide some clues why there are differences between the measured primary and the quarter-wave frequencies that are given in Table 1. The quarter wave frequency assumes that the waves within the tube in both compression and expansion phases are simple (i.e. spatially compact) acoustic or weak waves. It also assumes zero flow velocity within the tube. In reality, the waves in the compression phase can be assumed to be simple, in general, but this is not the case for the expansion phase. The presence of a plateau in the compression phase in Figure 16 for the longer tube and the lack of it in the expansion phase confirm this statement. Also, it is known that expansion waves will be acoustic waves, but the compression waves will have a speed higher than acoustic waves, in general, and only equal to it in the limit. Therefore, the time for the compression phase must be smaller or equal to that of the expansion phase, if the flow velocity within the tube was negligible. However, the results presented in Figure 16 for the deeper tube shows a longer compression phase, which highlights the effect of flow velocity. Both the expansion and compression waves traveling from the entrance of the tube toward the closed end of the tube encounter quiescent flow within the tube. However, in the return, the expansion waves ride on the flow, which is traveling in the same direction, while compression waves and the flow travel in the opposite directions.

In addition to its effect on the frequency, the tube depth affects the amplitude of the primary frequency peak for both the far-field acoustic and the near-field pressure. It was observed that as the frequency is decreased (or the tube depth is increased), the amplitude of the primary frequency peak is decreased as well. The reduction in amplitude is non-linear and appears to be leveling off towards the lower frequencies -- changing the tube depth from $1d$ to $2d$ has a more drastic effect than changing it from $3d$ to $6d$. The current results, which show that the amplitude is maximum at $L=1d$ is in agreement with the results of Savory²² who investigated this effect in great detail.

Jet Mach Number/Nozzle Pressure Ratio

In the current configuration, which uses a converging nozzle, the tonal frequencies appear only when the jet is operated in the underexpanded flow regime. The exit pressure of the nozzle is higher than the ambient pressure for this flow regime. To state the degree of underexpansion, one can either provide the ratio of stagnation pressure to ambient pressure or jet Mach number, which

is obtained by an hypothetical isentropic expansion of the flow from the given stagnation pressure to the ambient pressure. The latter is chosen here. The frequency contents of both near-field pressure and far-field acoustic measurements were obtained by FFT. Figures 18 and 19 show power spectra of acoustic and pressure signals for two cases with similar geometry (the tube depth and the separation distance of $1d$) but with different jet Mach Numbers ($M_j = 1.16$ and 1.33). Two main observations are the striking similarity of the tonal frequency content of near-field pressure and far-field acoustic signals and the strengthening of the primary peak along with the appearance of more subharmonics for the higher M_j case. One would expect the latter effects be due to the higher M_j , which would results in stronger compression and expansion waves. However, this could also be due to a better location for the entrance of the tube, as the compression/expansion pattern shifts as M_j is changed, while the geometry is fixed.

Another experiment was carried out to obtain the frequency content of the flow more locally (over a line), rather than globally such as that of pressure or acoustic. The beam of a He-Ne laser was passed through the flow before striking the surface of a photodetector. Figure 20 shows the FFT of the data for $L=\Delta x=1d$ and M_j of 1.33 . The laser beam was normal to the jet centerline and intersected it 3 mm downstream of the nozzle, half way between the nozzle and tube. The similarity of the frequency content in the flow (Fig. 20), far-field acoustic (Fig. 18b), and pressure (Fig. 19b) is striking. The He-Ne laser beam was traversed along the jet centerline of the HT looking for any dependence on measurement location. Only the amplitudes of the tonal features were altered with beam location while the frequency content remained unchanged.

Separation Distance

It was discussed earlier that the separation distance between the nozzle and tube has significant influence on the amplitude of primary oscillations, with $\Delta x = 1d$ providing the largest amplitude. In Figure 21 we present the range of required jet Mach numbers to achieve strong instabilities within the HT. The separation distance is plotted on the x-axis and each separation distance contains a series of jet Mach numbers for which strong oscillations were observed. The jet Mach number was varied between 1 and 1.8 (this is the range allowed by the setup). It is clear from the figure that as the separation distance is increased the required minimum M_j as well as the range of M_j 's for oscillations to occur is increased. Raman et al.⁵⁶ showed similar results for cylindrical, conical, and stepped tubes. These effects stem from the increase in the shock cell length as M_j is increased. Norum and Seiner⁵² presented the shock cell length (L_s) as a function of M_j and nozzle diameter (d) for a converging underexpanded nozzle as:

$$L_s = 1.1d\sqrt{M_j^2 - 1} \quad (7)$$

Increased operation range, which gives more flexibility, is obviously positive. However, increased minimum M_j is negative, as it increases the required mass flow rate.

Flow Visualization

Flow visualization was used to gain a better understanding of the flow field of the HT. If the HT is to be used as a fluidic actuator, it is crucial to understand its flow characteristics. Most researchers in the past have used schlieren or shadowgraph to study the flow of the HT (Thompson⁶², Kang⁴⁵, Solomon⁵⁸, Kawahashi and Suzuki⁴⁶, and Iwamoto and Deckker⁴⁴). These techniques have very poor spatial resolution, as they provide line-of-sight averaged images of the flow. Such images have provided useful information in nominally two-dimensional flows that are not highly turbulent. However, the HT flow is expected to be quite three-dimensional and highly

turbulent. Therefore, the planar flow visualization technique with a very short exposure time of 9 ns is much better suited for this flow.

Figure 22 shows a set of phase-averaged images at four equally spaced phases for a tube depth of $3d$, a separation distance of $2d$, and an M_j of 1.6. The nozzle is on the left and the tube is on the right in all the images. Only the upper half of the flow is visualized due to the partial blockage of the laser sheet by both the nozzle and the tube, as the laser sheet was brought in from the top. The mid compression and expansion phases are shown in images 22 (a) & (c), respectively. The images are equally spaced in time, 55 μ sec apart, throughout one cycle. During the expansion phase, images 22 (c) & (d), the flow out of the HT system is more inclined toward the tube, rather than 90° to the centerline of the nozzle/tube. Another characteristic of the flow is that in the compression phase, images 22 (a) & (b), not all the jet fluid is being entrained into the tube.

Figure 23 shows four instantaneous images, out of 60 used to get the phase-averaged image of 22 (d). Two main observations are that 1) the flow out of HT in the expansion phase contains both streamwise and spanwise structures, and 2) how deceptive the phase-averaged images are.

To explore the effects of M_j , the flow visualization results for the same geometry of Figure 22 but operating at an M_j of 1.3 are shown in Figure 24. This case has approximately 40% less mass flux than the previous one. Comparing images 22 (a) & (b) and 24 (a) & (b), there appears not to be much of a difference between the two flow fields for the compression phase. During the expansion phase, however, the images for the larger mass flow case show more fluid being ejected, as expected. Comparison of instantaneous images (Figures 23 & 25), does not reveal any major changes on the nature of the structures.

The importance of the separation distance between the nozzle and the tube was discussed earlier. To explore this effect on the flow characteristics, the tube depth and M_j were respectively held fixed at $3d$ and 1.3 as in Figures 24 & 25, but the separation distance was decreased from $2d$ to $1d$. The phase-averaged images for this case are shown in Figure 26, and four instantaneous images are shown in Figure 27. Recall that this is optimum separation distance for near-field pressure and far-field acoustic fluctuations. Three main differences can be seen between the images for the $1d$ and $2d$ cases, all of which are consistent with the pressure and acoustic results. First, the nozzle flow is pushed back farther for $1d$ case and the exiting jet has an angle of about 90° to the nozzle/tube centerline during the expansion phase. Second, more fluid is entrained into the tube, during the compression phase. Finally, the exiting jet contains larger undulations, indicating the presence of stronger turbulence structures.

Varying the tube depth was already shown to have a major impact on the primary frequency (Figure 25) and also on the percent of time spent in the compression phase (Figure 26 & Table 1). When the tube depth was varied, the flows for $1d$ and $3d$ tube depths did not show any major differences. This is consistent with the schlieren flow visualization results of Thompson.²⁷

Flow visualization was also performed on a HTFA configuration to better understand how adding a cylindrical shield between the nozzle and tube would affect the flow field generated by the HT. The experiments were performed at two separate M_j for three tube depths of $1d$, $2d$, and $3d$. The separation distance was held constant at 8mm for all the images. In all the images shown here, the nozzle is on the left, the tube is on the right, and the shield is on the lower part of the images extending between the nozzle and the tube. The area where the flow is visualized is at the open

area of the shield. This is the same location where the pulsating jet would be injected into a flow field to be controlled.

Figures 28 and 29 both present phase-averaged and instantaneous images for a tube depth of $3d$ and an M_j of 1.3. The time separation for all $3d$ tube depth images is 70 μsec . As expected, the compression phase (images 28 a & b) shows that not all the fluid is being entrained into the tube. The mid expansion phase (image 28 c) shows fluid being ejected into the ambient at 90° to the jet centerline near the injector, but as the fluid moves farther away, it begins to have a wavy appearance. The instantaneous images in Figure 29 also show this wavy appearance in the expansion phase, which seems to indicate the presence of strong vortical structures in the flow. The undulation shown on the phase-averaged image (image 28 a) in the expansion phase was not noticed in any of the phase-averaged images from the HT; therefore it either indicates the presence of strong and semi-spatially stationary vortical structures or it is a result of adding the shield. If it is due to the geometry, whether it is specific to this geometry or it is a general characteristic of HTFA is not clear at this time. The images for the same geometry but an M_j of 1.1 show similar characteristics, except for the effect of reduced mass flux that was discussed earlier for the HT.

Figures 30 and 31 present phase-averaged and instantaneous images for a tube depth of $2d$ and an M_j of 1.3. The time separation for all $2d$ tube depth images is 55 μsec . Again, the expansion phase has more fluid being ejected for the $3d$ case than $2d$ case. Since the tube depth of $3d$ is larger than the $2d$, it can entrain more fluid into the tube than the $2d$ case thus allowing it to have more fluid to eject during the expansion phase.

The HT and the HTFA operate under similar principles. However when the shield is added, the pulsating flow is concentrated in a smaller area, becomes more voluminous in the images, and possesses higher velocity and momentum. This is a very desirable feature for a fluid actuator in flow control. The flow for the HTFA during the expansion phase was always being ejected at an angle of 90° with respect to the jet centerline, which seems to be due to the nozzle and tube separation distance, as the HT had a pulsating jet at 90° only when the separation distance was $1d$. Another noticeable difference was that the presence an undulation in the phase-averaged flow for all the HTFA cases but never for any of the HT cases, the reason for which is not clear at this time.

II.4 SUMMARY

A Hartmann Tube was constructed that allowed for the examination of how various geometric parameters affected its performance. The geometric parameters included tube depth, separation distance, and the jet Mach number (strength of underexpansion). Dynamic pressure measurements in the near-field and microphone measurements in the far-field provided both temporal and spectral data to study the impact of the geometric parameters. Instantaneous and phase-averaged images of the flow allowed exploration into the nature of the turbulent structures within the flow.

The global near-field pressure, far-field acoustic, and flow results yielded similarities in both the frequency content and amplitude of the tonal frequency. Time traces of the pressure on the tube wall provided insight into the major differences between the primary frequency of the HT and the predicted quarter-wave frequency. Flow visualization results displayed a flow pulsating at the tonal frequency, which was very rich in vortical structures. They also showed the significant effect that the separation distance has on the direction of the pulsating jet out of HT, which would

play a major role in flow control. Flow visualizations were also taken of a Hartmann Tube based Fluidic Actuator. The flow from the HTFA was much more concentrated due to the addition of a shield between the nozzle and the tube. The flow results illustrate many similarities, but also some differences between HT and HTFA.

III: ACKNOWLEDGMENTS

This work was sponsored in part by the Air Force Office of Scientific Research, USAF, under grant/contract number F49620-97-1-0493. The views and conclusions contained herein are those of the authors and should not be interpreted as necessarily representing the official policies or endorsements, either expressed or implied, of the Air Force Office of Scientific Research or the U.S. Government. The work is also supported in part by NASA Glenn Research Center and a DAGSI grant (with AFRL/VA). The authors are also thankful for the assistance of David Benson, Marco Debiasi, William Erskine, James Hileman, Jason Petric, and Brian Thurow.

IV: REFERENCES

- ¹ Smith, M. J. T., "Aircraft Noise," Cambridge University Press, 1989.
- ² Lighthill, M. J., "On Sound Generated Aerodynamically: I. General Theory", Proceedings of the Royal Society of London, 1952, A 211, pp. 564-581.
- ³ Ffowcs-Williams, J. E., "The Noise from Turbulence Convected at High Speed", Phil. Trans. Roy. Soc., 1963, A255, pp. 469-503.
- ⁴ Ahuja, K. K. and Brown, W. H., "Shear Flow Control by Mechanical Tabs", AIAA Paper 1998, AIAA-89-0994.
- ⁵ Samimy, M., Zaman, K. B. M. Q., and Reeder, M. F., "Effects of Tabs on the Flow and noise Field of an Axisymmetric Jet", AIAA Journal, April 1993, Vol. 31, Mo. 4, pp. 609-619.
- ⁶ Rogers, C. B. and Parekh, D. E., "Mixing Enhancement by and noise Characteristics of Streamwise Vortices in an Air Jet", AIAA Journal, March 1994, Vol. 32, No. 3, pp. 464-471.
- ⁷ Surks, P., Rogers, C. B., and Parekh, D. E., "Entrainment and Acoustic Variations in a Round Jet from Introduced Streamwise Vorticity", AIAA Journal, October 1994, Vol. 32, No. 10, pp. 2108-2110.
- ⁸ Zaman, K. B. M. Q., Samimy, M., and Reeder, M. F., "Control of an Axisymmetric Jet Using Vortex Generators", Physics of Fluids 1994, Vol. 6, pp. 778.
- ⁹ Reeder, M. F. and Samimy, M., "The evolution of a Jet with Vortex-Generating Tabs: Real Time Visualization and Quantitative Measurements", Journal of Fluid Mechanics, 1996, Vol. 311, pp. 73-118.
- ¹⁰ Bohl D. G. and Foss, J. F., "Near Exit Plane Effects Caused by Primary and Primary-Plus-Secondary Tabs", AIAA Journal, February 1999, Vol. 37, No. 2, pp. 192-201.
- ¹¹ Tam, C. K. W. and Zaman, K. B. M. Q., "Subsonic Jet Noise from Non-Axisymmetric and Tabbed Nozzles", AIAA Paper 1999, AIAA-99-0077.
- ¹² Zaman, K. B. M. Q., "Jet Spreading Increase by Passive Control and Associated Performance Penalty", AIAA Paper 1999, AIAA-99-3505.
- ¹³ Ibrahim, M. K. and Nakamura, Y., "The Effects of Vane-Type Tabs on Flow and Acoustic Fields of Supersonic Jet", AIAA Paper 2000, AIAA 2000-0087.
- ¹⁴ Tam, C. K. W., "Subsonic Jet Noise from Nonaxisymmetric and Tabbed Nozzles", AIAA Journal, Vol. 38, No. 4, April 2000, pp. 592-599.
- ¹⁵ Gutmark, E., Schadow, K. C. and Bicker, C. J., "Near Acoustic Field and Shock Structure of Rectangular Supersonic Jets", AIAA Journal, July 1990, Vol. 28, No. 7, pp. 1163-1170.
- ¹⁶ Seiner, J. M., "Fluid Dynamics and Noise Emission Associated with Supersonic Jets", pp. 297-323, in Studies in Turbulence, 1991, Gatski, B., Sarkar, S., Speziale, C. G. (Ed.).

- ¹⁷ Kinzie, K. W. and McLaughlin, D. K., "An Experimental Study of Noise Radiated from Supersonic Elliptic Jets", AIAA Paper, 1995, AIAA-95-0511.
- ¹⁸ Raman, G., "Screech Tones from Rectangular Jets with Spanwise oblique Shock-Cell Structures", *Journal of Fluid Mechanics*, 1997, Vol. 330, pp. 141-168.
- ¹⁹ Tam, C. K. W., "Influence of Nozzle Geometry on the Noise of High-Speed Jets", *AIAA Journal*, August 1998, Vol. 36, No. 8, pp. 1396-1400.
- ²⁰ Tam, C. K. W., "Subsonic Jet Noise from Nonaxisymmetric and Tabbed Nozzles", *AIAA Journal*, Vol. 38, No. 4, April 2000, pp. 592-599.
- ²¹ Wlezien, R. W. and Kibens, V., "Influence of Nozzle Asymmetry on Supersonic Jets", *AIAA Journal*, January 1988, Vol. 26, No. 1, pp. 27-33.
- ²² Rice, E. J. and Raman, G., "Mixing Noise Reduction for Rectangular Supersonic Jets by Nozzle Shaping and Induced Screech Mixing", AIAA Paper, 1993, AIAA-93-4322.
- ²³ Samimy, M., Kim, J.-H., Clancy, P. S., and Martens, S., "Passive Control of Supersonic Rectangular Jets via Nozzle Trailing Edge Modifications", *AIAA Journal*, 1998, Vol. 36, pp. 1230.
- ²⁴ Kim, J.-H. and Samimy, M., "Mixing Enhancement via Nozzle Trailing Edge Modifications in a high Speed Rectangular Jet", *Physics of Fluids*, 1999, Vol. 11, No. 9, pp. 2731-2742.
- ²⁵ Verma, S. B. and Rathakrishnan, E., "Investigation of the Effect of Notch Geometry Variation on the Flow and Acoustic Field of Axisymmetric Jets", 3^d ASME/JSME Joint Fluids Engineering Conference, 1999, FEDSM99-6915.
- ²⁶ Kim, J.-H. and Samimy, M., "On Mixing Enhancement via Nozzle Trailing Edge Modifications in a high Speed Jet", *AIAA Journal*, 2000, Vol. 38, No. 5, pp. 935-937.
- ²⁷ Kerechanin II, C. W., Samimy, M. and Kim, J.-H., "Effects of Nozzle Trailing Edge Modifications on Noise Radiation in a Supersonic Rectangular Jet", AIAA Paper, 2000, AIAA-2000-0086.
- ²⁸ Kerechanin II, C. W., "The Effects of Nozzle Trailing Edge Modifications on the Acoustic Far Field of a Mach 2 Rectangular Jet," Masters Thesis, Department of Mechanical Engineering, The Ohio State University, 2000.
- ²⁹ Hileman, J. I., "An Attempt at Identifying Noise Generating Turbulent Structures in a Mach 1.3 Axisymmetric Jet", Masters Thesis, Department of Mechanical Engineering, The Ohio State University, 2000.
- ³⁰ Hileman, J. and Samimy, M., "An Attempt to Identify Noise Generating Turbulent Structures in a High Speed Axisymmetric Jet," AIAA Paper, 2000, AIAA-2000-2020.
- ³¹ Duda, J., "Inverse Square Law Measurements in Anechoic Rooms", *Journal of Sound and Vibration*, December 1998, pp. 20-25.

- ³² Tanna, H. K., "An Experimental Study of Jet Noise Part II: Shock Associated Noise," *Journal of Sound and Vibration*, Vol. 50, 1977, pp. 429-444.
- ³³ Tam, K. W., "Supersonic Jet Noise," *Annual Review of Fluid Mechanics*, Vol. 27, 1995 pp. 17-43.
- ³⁴ Seiner, J. M., "Advances in High Speed Aeroacoustics", AIAA Paper, 1984, AIAA-84-2275.
- ³⁵ Harper-Bourne, M. and Fisher, M. J., "The Noise from Shock Waves in Supersonic Jets", AGARD-CP-131, AGARD, Neuilly-Sur-Seine, France, 1974, pp. 11-1 to 11-13.
- ³⁶ Brocher, E., Maresca, C., and Bournay, M.-H., "Fluid Dynamics of the Resonance Tube," *J. Fluid Mech.*, Vol. 43, Part 2, 1970, pp 369-384.
- ³⁷ Brocher, E., and Ardissonne, J-P., "Heating Characteristics of a new type of Hartmann-Sprenger tube," *Int. J. Heat and Fluid Flow*, Vol. 4, No. 2, 1983, pp 97-102.
- ³⁸ Brown, G.L. and Roshko, A., "On Density Effects and Large Structure in Turbulent Mixing Layers," *J. Fluid Mech.*, Vol. 64, 1974, pp.715-816
- ³⁹ Crow, S.C. and Champagne, F.H., "Orderly Structure in Jet Turbulence," *J. Fluid Mech.*, Vol. 48, 1971, pp 547-591
- ⁴⁰ Hartmann, J., and Trolle, B., "A New Acoustic Generator," *J. Sci. Instr.*, Vol. 4, 1927, pp 101-111.
- ⁴¹ Hartmann, J., "Construction, Performance, and Design of the Acoustic Air-Jet Generator," *J. Sci. Instr.*, Vol. 16, 1939, pp 140-149.
- ⁴² Ho, C-M and Huang, L-S, "Subharmonics and Vortex Merging in Mixing Layers," *J. Fluid Mech.*, Vol. 119, 1982, pp 443-473
- ⁴³ Ho, C-M, and Huerre, P., "Perturbed Free Shear Layers," *Ann. Rev. Fluid Mech.*, Vol. 16, 1984, pp. 365-424
- ⁴⁴ Iwamoto, J., and Deckker, B.E.L., "A Study of the Hartmann-Sprenger Tube Using the Hydraulic Analogy," *Exp. in Fluids*, Vol. 3, 1985, pp 245-252.
- ⁴⁵ Kang, S.W., "Resonance Tubes," Ph.D. thesis, 1964, Rensselaer Polytechnic Institute, Troy, N.Y.
- ⁴⁶ Kawahashi, M., and Suzuki, M., "Generative Mechanism of Air Column Oscillation in a Hartmann-Sprenger Tube Excited by an Air Jet Issuing from a Convergent Nozzle," *J. Appl. Math and Phys.*, Vol. 30, 1979, pp. 797-810.
- ⁴⁷ Kawahashi, M., Bobone, R., Brocher, E., " Oscillation Modes in Single-Step Hartmann-Sprenger Tubes," *J. of the Acoustical Society of America*, Vol. 75, No. 3, 1984, pp 780-784.

- ⁴⁸ Kibens, V., "Discrete Noise Spectrum Generated by an Acoustically Excited Jet," AIAA J., Vol. 18, April 1980, pp 434-441
- ⁴⁹ Kibens, V., Dorris III, J., Smith, D.M., and Mossman, M.F., "Active Flow Control Technology Transition: The Boeing ACE Program," AIAA 99-3507
- ⁵⁰ Marchese, V. P., Rakowsky, E. L., Bement, L. J., "A Fluidic Sounding Rocket Motor Ignition System," J. Spacecraft, Vol. 10, No. 11, 1973, pp 731-734.
- ⁵¹ Morch, K.A., "A Theory for the Mode of Operation of the Hartmann Air Jet Generator," J. Fluid Mech., Vol. 20, Part 1, 1964, pp. 141-159.
- ⁵² Norum, T.D., and Seiner, J.M., "Broadband Shock Noise from Supersonic Jets," AIAA J. Vol. 20. No. 1, 1982, pp. 68-73
- ⁵³ Parekh, D.E., Kibens, V., Glezer, A., Wiltse, J.M., and Smith, D.M., "Innovative Jet Flow Control: Mixing Enhancement Experiments," AIAA 96-0308.
- ⁵⁴ Raman, G., Kibens, V., Cain, A., and Lepicovsky, J., "Advanced Actuator Concepts for Active Aeroacoustic Control," AIAA 2000-1930.
- ⁵⁵ Raman, G., and Kibens, V., "Active Flow Control Using Integrated Powered Resonance Tube Actuators," AIAA 2001-3024
- ⁵⁶ Raman, G., Mills, A., Othman, S., and Kibens, V., "Development of Powered Resonance Tube Actuators for Active Flow Control," ASME FEDSM 2001-18273
- ⁵⁷ Savory, L.E., "Experiments with the Hartmann Acoustic Generator," Engineering, Vol. 170, Aug. 1950, pp 99, 100, 136-138.
- ⁵⁸ Solomon, L., "Hydraulic Analogue Study of the Hartmann Oscillator Phenomenon," J. Fluid Mech., Vol. 28, Part 2, 1967, p. 261-271.
- ⁵⁹ Sprenger, H., "Ueber thermische Effekte in Resonanzrohren," Fed. Inst. Tech., Zurich, Vol. 21, 1954, pp. 18-35.
- ⁶⁰ Stanek, M.J., Raman, G., Kibens, V., and Ross, J., "Control of Cavity Resonance Through Very High Frequency Forcing," AIAA 2000-1905.
- ⁶¹ Stanek, M.J., Raman, G., Kibens, V., Ross, J.A., Odedra, J., and Peto, J.W., "Suppression of Cavity Resonance Using High Frequency Forcing-The Characteristic Signature of Effective Devices," AIAA 2001-2128
- ⁶² Thompson, P., "Jet-Driven Resonance Tube," AIAA J., Vol. 2, No. 7, July 1964, pp. 1230-1233
- ⁶³ Winant, C.D. and Browand, F.K., "Vortex Pairing: The Mechanism of Turbulent Mixing-Layer Growth at Moderate Reynolds Number," J. Fluid Mech., Vol. 63, p. 237, 1974

V. TABLES

Table 1. Fundamental and quarter-wave frequencies and percentage duration of compression and expansion phases in a cycle for various tube depth				
<i>L</i> (Tube depth)	<i>1d</i>	<i>2d</i>	<i>3d</i>	<i>6d</i>
¼ Wave Freq. (kHz)	14.4	7.2	4.8	2.4
Min. Freq. (kHz)	7.4	4.7	3.2	2.0
% Difference	49%	35%	33%	17%
Max. Freq. (kHz)	9.4	5.6	4.1	2.6
% Difference	35%	22%	15%	8%
% Time in Comp.	52%	59%	61%	64%
% Time in Expan.	48%	41%	39%	36%

VI: FIGURES

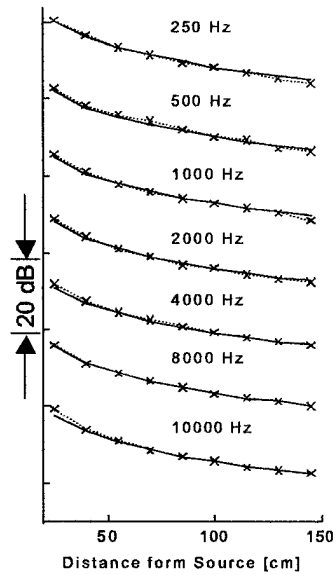
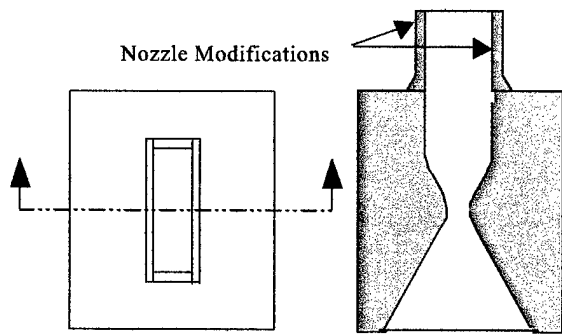
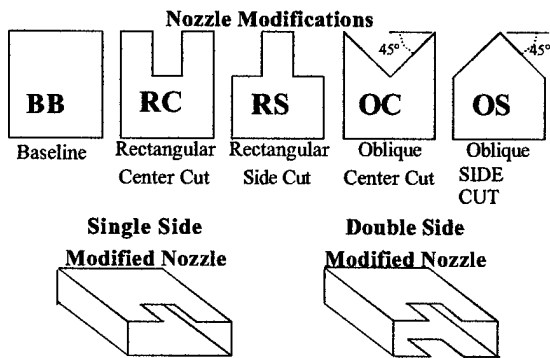


Figure 1 One of the eight microphone paths in the chamber showing the decay of the SPL measured (-x-) compared to that of the theoretical curve (-) at various frequencies.



a. The nozzle block. Notice the location of the nozzle modifications. Not to scale.



b. The nozzle modifications, notice the abbreviations in each diagram, and the single side (asymmetric) and double side modified (symmetric) cases. Not to scale.

Figure 2 Nozzle modifications used in the study.

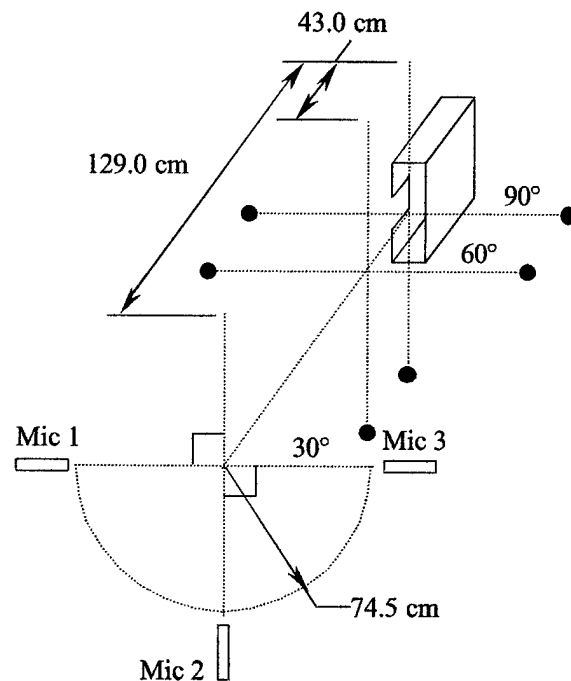


Figure 3 Positions of the microphones.

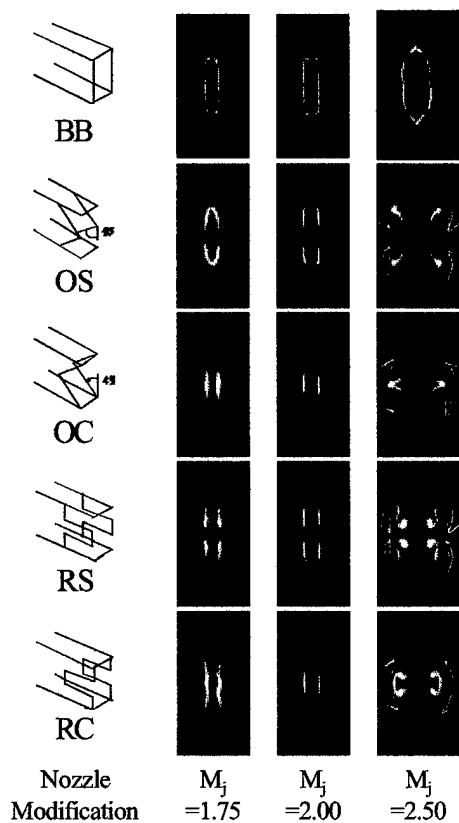


Figure 4 Visualization of jet cross section at 1 equivalent jet diameter downstream of the nozzle exit for over, ideally and under expanded flow regimes with various nozzles.²⁴

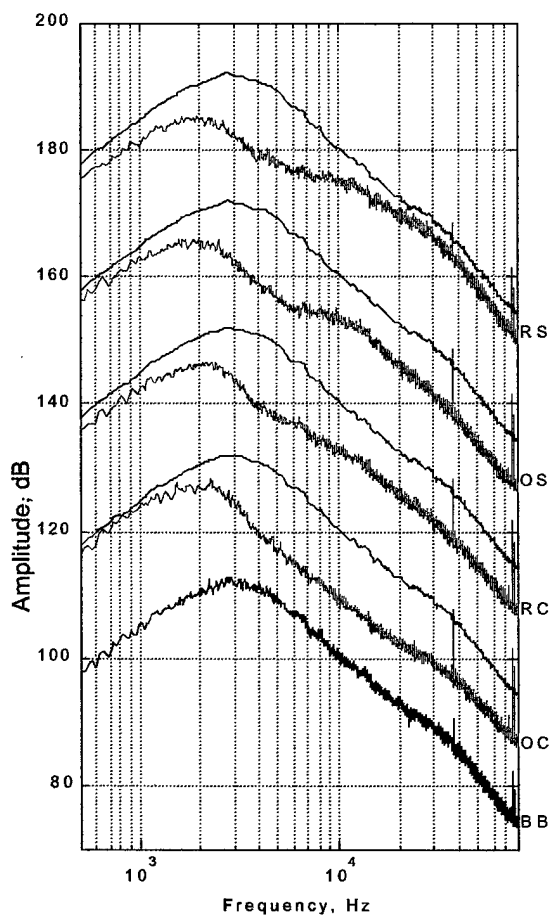


Figure 5 Spectra from microphone 1 for the double side nozzle modifications as compared to the baseline case for the underexpanded flow condition measured at 30°. Each spectrum has been upshifted by 20dB.

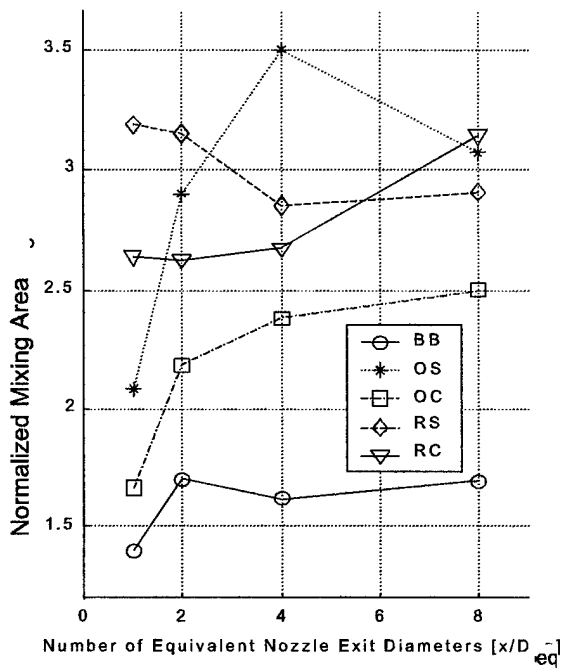


Figure 6 Normalized-mixing area results for the underexpanded flow of the double side modified nozzle configurations.²⁴

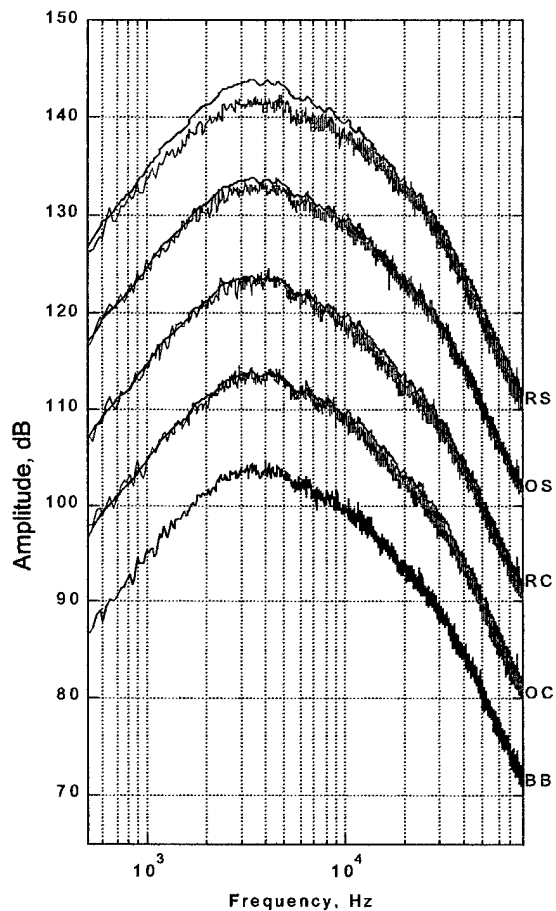


Figure 7 Spectra from microphone 1 for the single side nozzle modifications as compared to the baseline case for the ideally expanded flow condition measured at 30°. Each spectrum has been upshifted by 10dB.

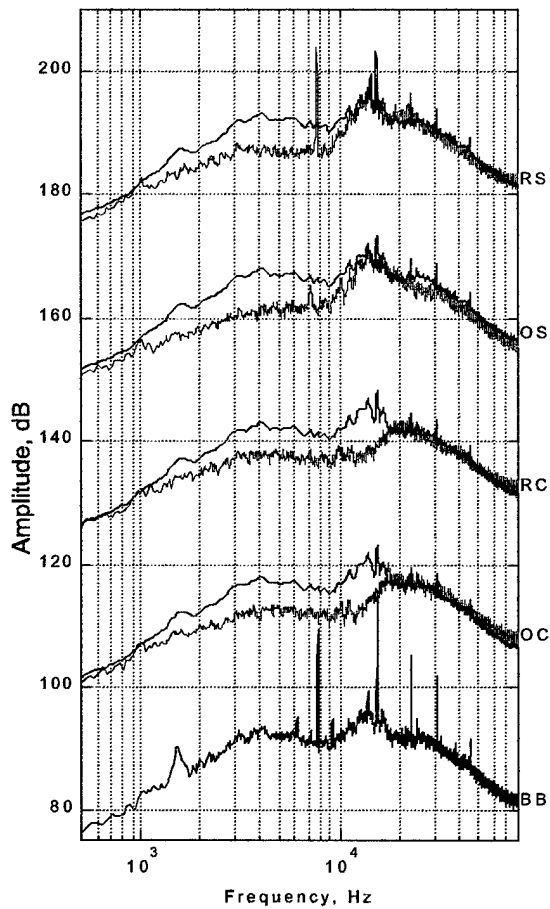


Figure 8 Spectra from microphone 1 for the single side nozzle modifications as compared to the baseline case for the over expanded flow condition measured at 90°. Each spectrum has been upshifted by 25dB.

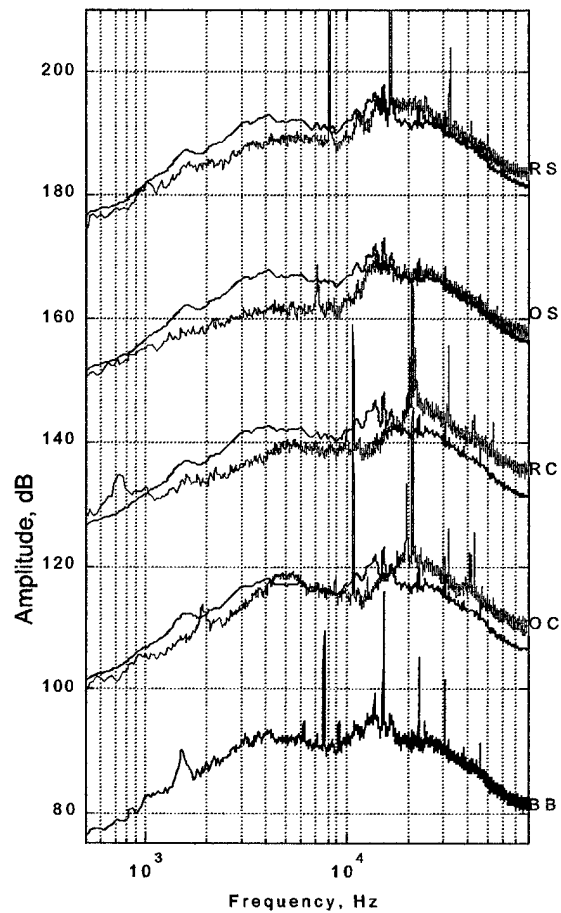


Figure 9 Spectra from microphone 1 for the double side nozzle modifications as compared to the baseline case for the over expanded flow condition measured at 90°. Each spectrum has been upshifted by 25dB.

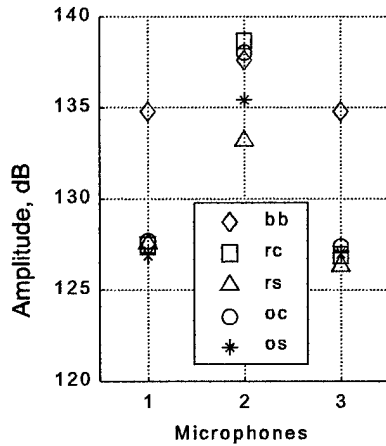


Figure 10 The OASPL as calculated for the three microphones in the underexpanded flow regime, double side modified nozzle at 30°.

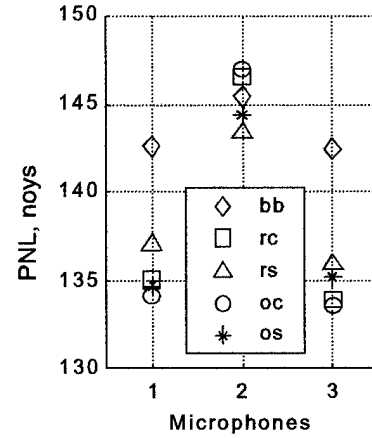
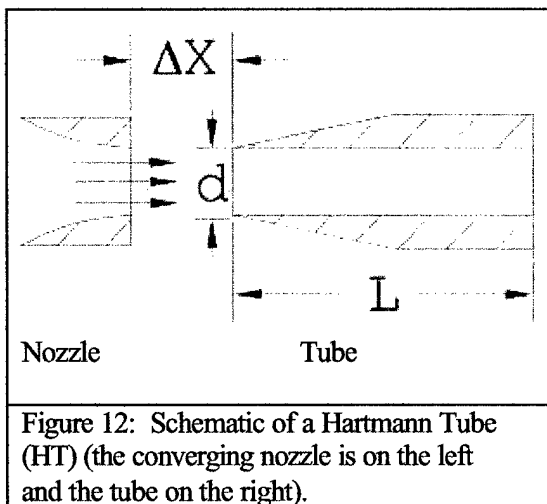


Figure 11 The PNL as calculated for the three microphones in the overexpanded flow regime, double side modified nozzle at 30°.



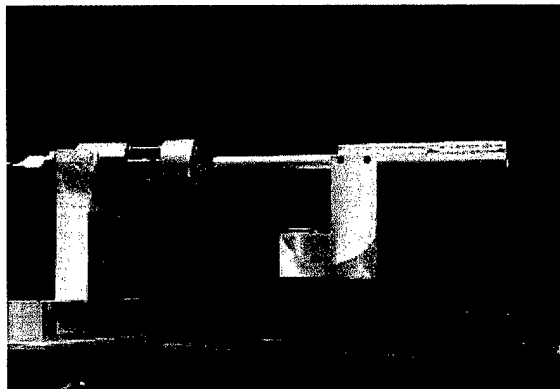


Figure 13. A photograph of the HT set up

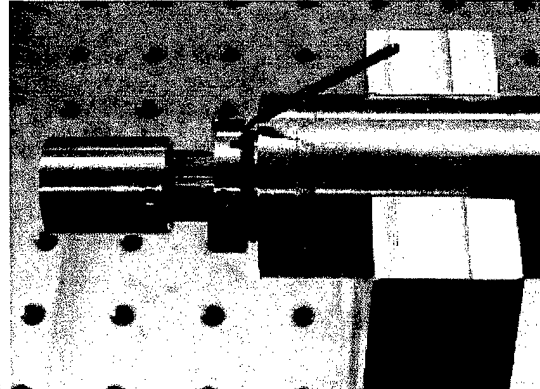


Figure 14. A photograph of a HT based Fluidic Actuator (HTFA)

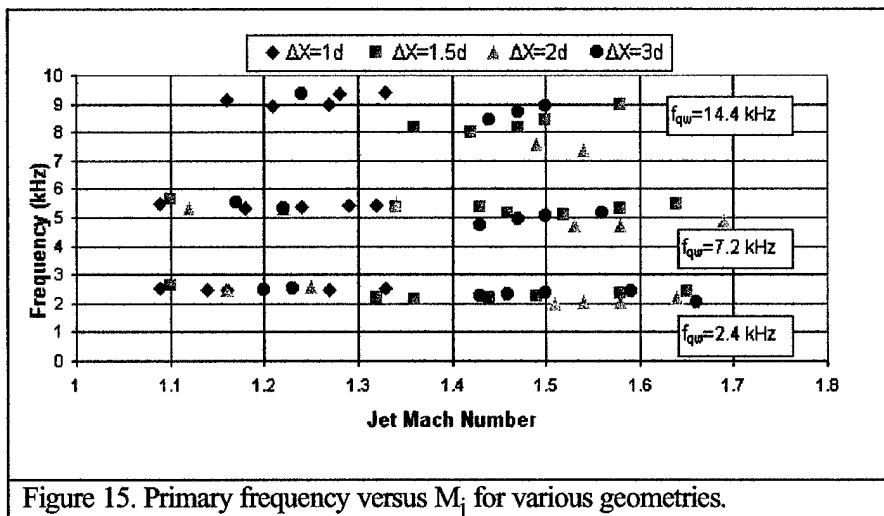


Figure 15. Primary frequency versus M_j for various geometries.

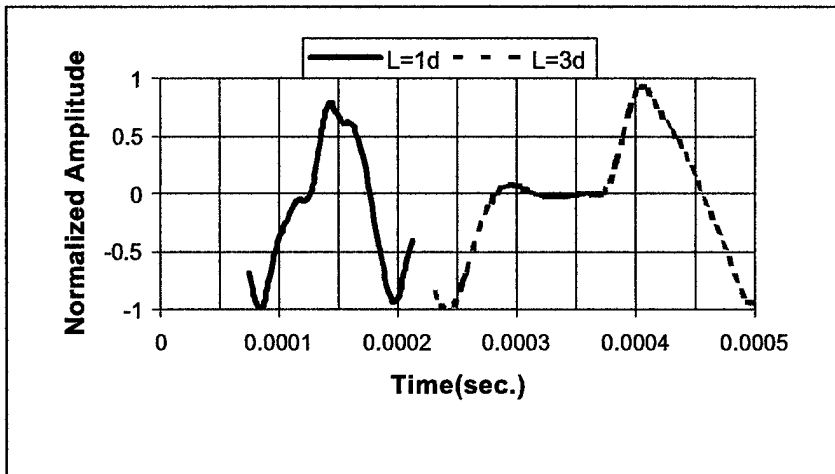


Figure 16. Time traces for two tube depths ($\Delta x=1d$, $M_j=1.1$ & $M_j=1.2$ for shorter and longer tubes).

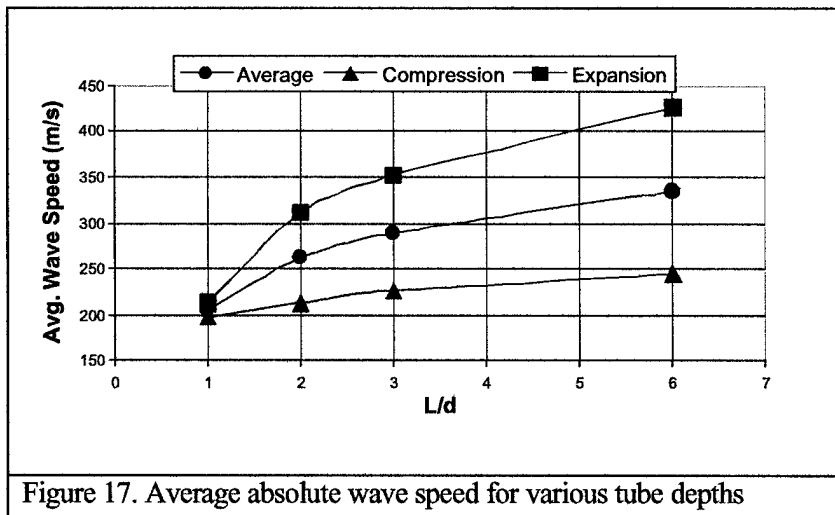


Figure 17. Average absolute wave speed for various tube depths

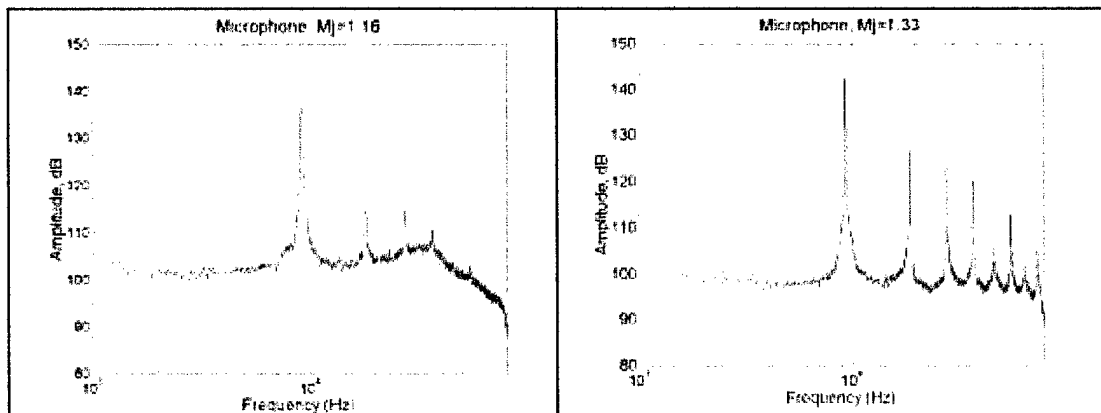


Figure 18. Power spectra of far-field acoustic signal for two jet Mach numbers, at a fixed geometry of $L=1d$ and $\Delta x=1d$

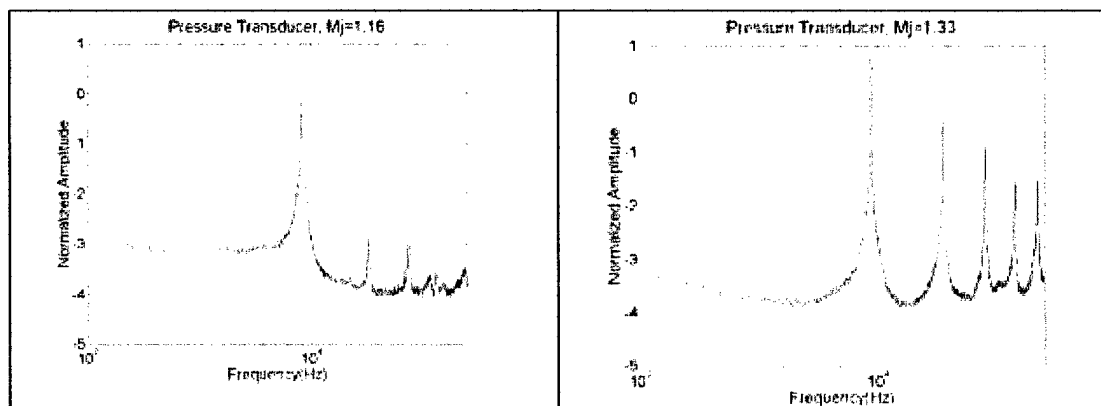
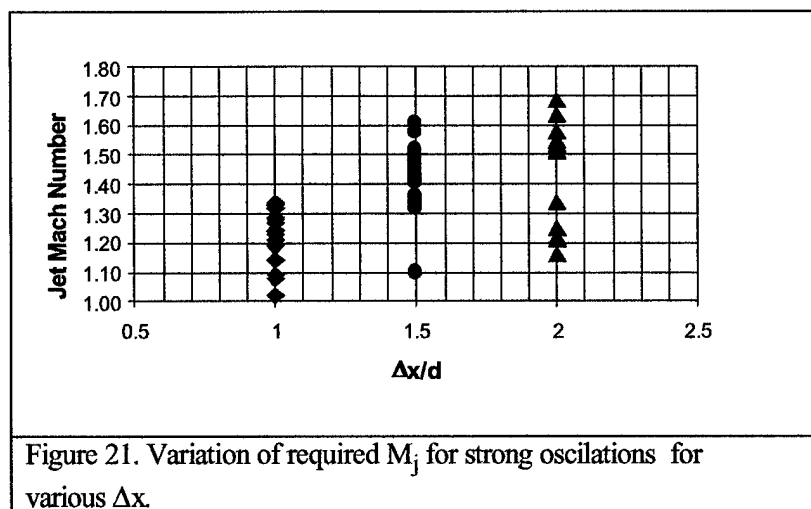
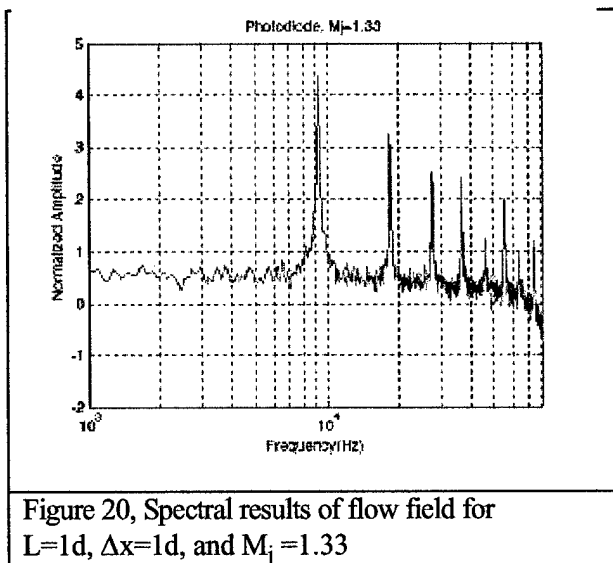


Figure 19. Power spectra of near-field pressure signal for two jet Mach numbers, with same geometry as in Figure 7.



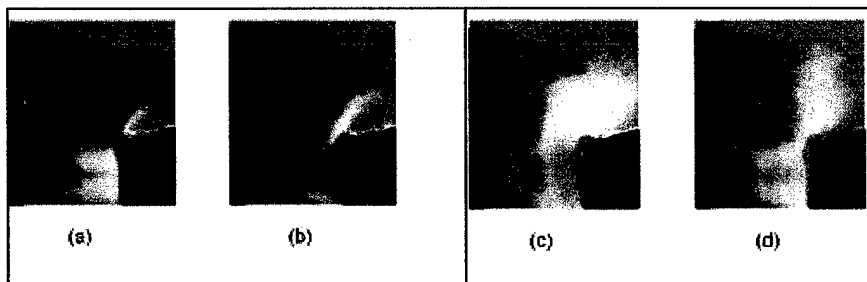


Figure 22. Phase-averaged flow images for $L=3d$, $\Delta x=2d$, $M_j=1.6$; compression phase (a & b) and expansion phase (c & d)

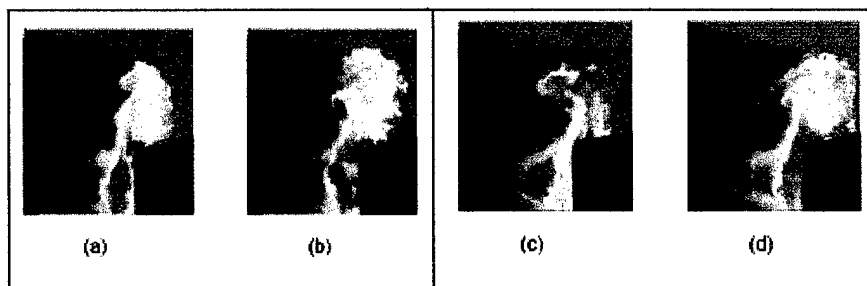


Figure 23. Instantaneous images for Figure 11 d.

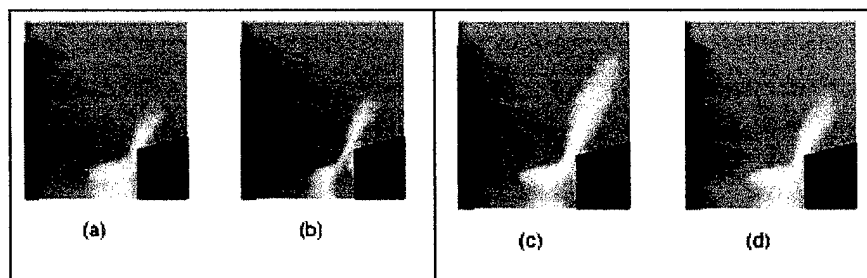


Figure 24. Phase-averaged flow images for $L=3d$, $\Delta x=2d$, $M_j=1.3$; compression phase (a & b) and expansion phase (c & d)

